Power Electronic Systems
Laboratory

Proceedings of the 19th IEEE Workshop on Control and Modeling for Power Electronics (COMPEL 2018),
Padova, Italy, June 25-28, 2018

Optimal Design of Highly Efficient and Highly Compact PCB Winding Inductors

J. Schäfer,
D. Bortis,
J. W. Kolar

Eidgenössische Technische Hochschule Zürich
Swiss Federal Institute of Technology Zurich

Optimal Design of Highly Efficient and Highly Compact PCB Winding Inductors

Jannik Schäfer, Dominik Bortis and Johann W. Kolar
Power Electronic Systems Laboratory
ETH Zurich
Physikstrasse 3, 8092 Zurich, Switzerland
Email: schaefer@lem.ee.ethz.ch

***Abstract*—In industrial power electronic systems, power density and costs are key design criteria. Therefore, very high switching frequencies are commonly used in order to minimize the volume of the inductive components. However, especially in high-current applications, the well-known skin and proximity effects as well as the fringing field around the air gaps of inductors, impede the design of these components, as they are usually all reducing the effective cross-sectional area of solid inductor windings. Consequently, litz wire windings would have to be used, which is often impossible, mainly due to cost reasons. This paper introduces a new, simple and efficient approach on how to integrate inductor windings directly into the PCB, by mitigating the high-frequency losses due to a relocation of the air gap. In this way, its fringing field can be used to partly compensate the parasitic magnetic fields causing the skin and proximity effects. Hence, very low production costs and high power densities can be achieved. In a first step, simple design guidelines are derived and verified by means of simulations. Finally, a possible hardware implementation of the proposed concept is presented.**

***Index Terms*—PCB inductor, air gap relocation, magnetic field compensation**

I. Introduction

Inductors are used in a variety of electronic applications and especially in the area of power electronic converter systems, where they are usually employed as filter components in order to attenuate the switching frequency output voltage ripple, e.g. of buck converter topologies [1] [2]. Hence, the inductive components need to be designed in such a way that they can handle a certain required maximum output current, whereby an appropriate copper cross-section of the winding needs to be provided in order to limit the arising conduction losses in the inductor winding. However, especially in high-power low-voltage applications, these inductor currents can be huge and therefore large copper cross-sections A_{cu}, e.g. using wide copper bars and solid conductor windings, are required. To achieve a high power density, it is therefore important to obtain a homogeneous current density throughout A_{cu}, in order to optimally use the employed copper material and therefore maximize the effective copper cross-sectional area $A_{\mathrm{cu,eff}}$ of the winding.

However, a homogeneous current density is difficult to achieve, since due to the high-frequency (HF) current components resulting from the switching frequency, different parasitic effects come into play, which deflect the current towards the surface or edges of the conductor and thereby reduce the effective $A_{\mathrm{cu,eff}}$. These parasitic HF effects can be divided into three main components: First, the skin effect, which characterizes the impact of the magnetic field H_{skin} of a HF current in a conductor on its own conductivity, second, the proximity effect, which describes the mutual influence of the magnetic fields H_{prox} of multiple current carrying conductors on their individual current distributions and lastly the third component, which originates from the impact of the fringing field H_{ag} around an air gap of the magnetic circuit on conductors in its near vicinity [3]. Hence, if H_{ag} penetrates a conductive material, it induces eddy currents according to the well-known law of induction and therefore acts similar to the aforementioned proximity effect (cf. **Fig. 1**).

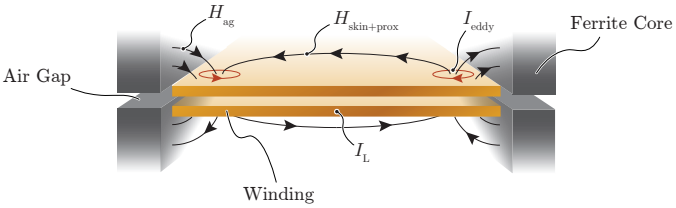

Fig. 1. Parasitic magnetic fields $H_{\mathrm{skin+prox}}$ and H_{ag} in a conventional arrangement of a PCB winding inductor, which are inducing eddy currents I_{eddy} in the conductor and therefore increase the total conduction losses.

These effects can be minimized in wire-wound inductors using litz wire, where multiple insulated thin copper strands are twisted in prescribed patterns, such that the flux linkages of all strands are equalized. As a result, the current splits equally among the individual wire strands and due to their much smaller wire diameter the skin effect caused by H_{skin} and the induced currents due to H_{prox} and H_{ag} in each strand can strongly be reduced [4]–[6].

Unfortunately, litz wire has some significant drawbacks compared to solid copper conductors. On the one hand, the copper fill factor is comparably poor, as a significant amount of the available wire cross-sectional area is wasted due to the spaces between the strands and the required insulation of each individual strand. On the other hand, the allowable

978-1-5386-5541-2/18/$31.00 ©2018 IEEE

current density in litz wire is strongly limited due to its large thermal resistance orthogonal to the wire surface [7]. In cost driven applicatiosn, however, the most significant downside of litz wire windings is their price, since the costs per weight of litz wire are much higher than the ones of solid conductors [8]. Furthermore, the wire wrapping process and the termination of these windings are challenging and also increase the manufacturing costs.

In industrial applications, solid conductor windings, and especially PCB integrated windings, are therefore preferred, as they allow for much higher current densities (improved power density) and a cheap and simple manufacturing of inductors. However, as already mentioned, large conductive surfaces are prone to induced eddy currents due to external magnetic fields. For this reason, different approaches have been presented in literature, which all try to minimize the external magnetic fields penetrating the conductor. The most efficient approaches use two different concepts: The first option is to reduce the fringing field of the air gap by means of either using multiple smaller air gaps (quasidistributed air gap, cf. **Fig. 2a**) or by using a low permeability material (true distributed air gap, cf. **Fig. 2b**) [9]. Another possibility is to place the air gaps perpendicular (z-direction) to the conductor, such that the main component of the resulting fringing field is heading into x-direction and therefore does not penetrate the conductor perpendicular to its surface, i.e. in z-direction. Consequently, the HF losses due to the fringing field of the air gap can be minimized, as long as the distance between the air gap and the conductor is larger than a certain value [9].

However, the manufacturing of inductor cores with multiple air gaps and/or low permeability material is difficult and expensive, which is why a design with a single air gap is usually preferred in industrial applications. Furthermore, in the aforementioned considerations, the influence of the existing perpendicular skin and proximity fields are usually neglected, even though they lead to significant HF losses in a real conductor. For this reason, in this paper these fields are taken into account as well, in order to end up with an optimized inductor geometry that ensures an almost frequency-independent current distribution and therefore optimal utilization of the cross section of the conductor. Thus, minimal HF losses in the windings and a high suitability for real implementations in efficient, powerdense and cost driven applications are obtained. In Section II, all aforementioned magnetic field components are derived by means of analytical and numerical calculations and based on these derivations, a simple field compensation concept is introduced, which allows for partial active compensation of the skin and proximity fields in a straight conductor using the fringing field of a single air gap placed perpendicularly to the conductor (cf. **Fig. 2c**). Hence, the AC resistance can be kept almost at the level of the DC resistance even for very high frequencies. In Section III, the concept is applied to a more practice-oriented circular conductor arrangement (cf. **Fig. 2d**) and simple design guidelines are provided. In Section IV, the influence of multiple parallel PCB layers on the applicability of the proposed concept is investigated in detail and an exemplary practical implementation of a PCB winding inductor is shown. Finally, Section V concludes the findings of this paper.

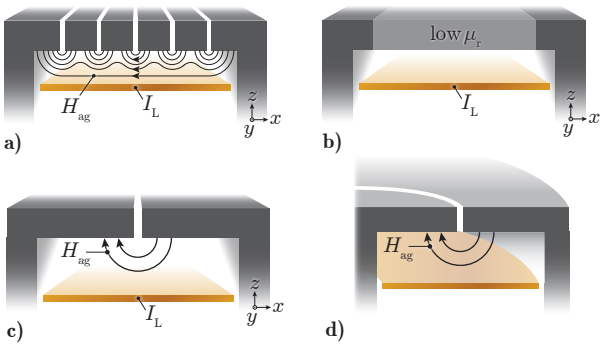

Fig. 2. Different air gap arrangements to reduce the conduction losses in PCB windings; e.g. **a)** multiple air gaps placed in parallel, i.e. in x-direction, along a straight conductor; **b)** distributed air gap using low permeability material. In **c)** and **d)**, single air gap arrangements along a straight and a circular conductor are shown.

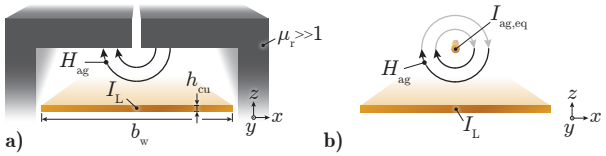

Fig. 3. a) Single air gap arrangement with the fringing field H_{ag} and **b)** its equivalent circuit where the fringing field H_{ag} is assumed to be induced by an equivalent current $I_{\mathrm{ag,eq}}$.

II. Field Compensation in Straight Conductors

The main challenge in the design of a highly efficient high-frequency (HF) inductor winding is the minimization of its AC resistance R_{AC}, which is the same as striving for an AC to DC resistance factor F_{R} close to one:

$$F_{\mathrm{R}} = \frac{R_{\mathrm{AC}}}{R_{\mathrm{DC}}} \xrightarrow{\text{minimize}} F_{\mathrm{R,opt}} = 1. \tag{1}$$

Hence, assuming $F_{\mathrm{R}} = 1$ and according to

$$P_{\mathrm{cond}} = R_{\mathrm{DC}} F_{\mathrm{R}} I_{\mathrm{rms}}^2 = \int_{\mathrm{V}} \frac{J(x,y,z)^2}{\sigma} \mathrm{d}V, \tag{2}$$

the conduction losses in the winding do not change with frequency, what inherently implies that the current distribution $J(x,y,z)$ in a conductor should be frequency-independent as well. Thus, independent of the actual inductor geometry, the AC current density J_{AC} should be equal to its DC equivalent J_{DC} in order to minimize the AC-resistance R_{AC} and therefore also the conduction losses. However, this is usually difficult to achieve, as various magnetic field components summarized to $\vec{H}_{\mathrm{eddy}}$ penetrate the conductor and induce eddy currents according to

$$\nabla \times \vec{E} = -\mu_0 \frac{\partial \vec{H}_{\mathrm{eddy}}}{\partial t}, \tag{3}$$

wherefore a current displacement and increased F_R values result.

In the following, the different field components contained in $\vec{H}_\mathrm{eddy}$ are analyzed based on the example arrangement of **Fig. 3a**, and their effects on the current distribution $J(x, y, z)$ are discussed.

The considered geometrical arrangement comprises an infinitesimally long straight conductor, surrounded by a ferrite core with a single air gap perpendicularly arranged to the top surface of the conductor, as illustrated in **Fig. 3a**. The corresponding DC current density can be calculated according to

$$J_\mathrm{DC}(x, z) = \frac{I_\mathrm{L}}{h_\mathrm{cu} \cdot b_\mathrm{w}} \cdot \vec{e}_\mathrm{y}, \tag{4}$$

where h_cu denotes the thickness and b_w the width of the copper track. However, in order to simplify the calculation of the various field components of $\vec{H}_\mathrm{eddy}$, it is assumed that the thickness h_cu of the conductor is smaller than the skin depth of the considered frequency f_sw, whereby even for high-frequency currents a homogeneous current density in z-direction results. This assumption is usually valid for PCB integrated inductor windings, where the copper thickness of the PCB with $35\,\mu\mathrm{m}..70\,\mu\mathrm{m}$ is smaller than the skin depth. Thus, an equivalent line current density J_line can be defined according to

$$J_\mathrm{line}(x) = h_\mathrm{cu} \cdot J_\mathrm{DC}(x) = \frac{I_\mathrm{L}}{b_\mathrm{w}} \cdot \vec{e}_\mathrm{y}, \tag{5}$$

emulating a current sheet with $h_\mathrm{cu} \to 0$. In order to achieve the desired $F_\mathrm{R} = 1$, the same constant line current density obtained with DC currents should also be achieved for HF currents, requiring zero time-varying magnetic field inside the conductor, as otherwise a current displacement would result (cf. (3)).

However, in the inductor arrangement at hand, there are always two main magnetic field components penetrating the conductor in z-direction. On the one hand, the magnetic skin field $H_\mathrm{z,skin}$ (cf. **Fig. 4a**), which originates from the current in the conductor and can be calculated according to Ampere's Law

$$\begin{aligned} H_\mathrm{z,skin}(x) &= \int_{\frac{-b_\mathrm{w}}{2}}^{\frac{b_\mathrm{w}}{2}} \frac{J_\mathrm{line}}{2\pi(\alpha - x)} d\alpha \\ &= \frac{I_\mathrm{L}}{2\pi b_\mathrm{w}} \left(\ln\left(x + \frac{b_\mathrm{w}}{2} \right) - \ln\left(\frac{b_\mathrm{w}}{2} - x \right) \right) \cdot \vec{e}_\mathrm{z}. \end{aligned} \tag{6}$$

On the other hand, the fringing field H_ag around the air gap, which can be derived according to [10], or for small air gaps even easier based on **Fig. 3b**, where the fringing field is assumed to be generated by an equivalent current $I_\mathrm{ag,eq} \approx 2I_\mathrm{L}$ [11]. The z-component of this magnetic field can therefore be calculated according to

$$H_\mathrm{z,ag}(x) = \frac{I_\mathrm{L}}{\pi} \cdot \frac{x}{d_\mathrm{w}^2 + x^2} \cdot \vec{e}_\mathrm{z}, \tag{7}$$

as shown in **Fig. 4a**. As can be noticed, both field components $H_\mathrm{z,skin}$ and $H_\mathrm{z,ag}$ are heading into opposite directions, whereby a partial mutual compensation of these fields can be observed. Consequently, the fringing field H_ag of the air gap counteracts the field of the skin effect H_skin, as the total magnetic field perpendicular to the conductor can be reduced

$$H_\mathrm{z,tot}(x) = H_\mathrm{z,skin}(x) + H_\mathrm{z,ag}(x). \tag{8}$$

However, as illustrated in **Fig. 4b**, the quality of the compensation, i.e. the distribution of the current density J_y, highly depends on the distance d_w between the conductor and the air gap, as for very small values of d_w, $H_\mathrm{z,ag}$ overcompensates $H_\mathrm{z,skin}$, whereby most of the current is attracted towards the middle of the conductor (dominating proximity effect), and for large values of d_w an undercompensation results and the current is pushed towards the edges of the conductor (dominating skin effect). Hence, there is an optimum distance $d_\mathrm{w,opt}$, where an almost homogeneous current distribution can be achieved and therefore a very low F_R value close to one results.

There are different approaches to find this optimum value of d_w, as e.g. the finite element method (FEM), where the geometric arrangement of **Fig. 3a** is simulated for different values of d_w and different frequencies f_sw. The resulting AC to DC resistance factors F_R are shown in **Fig. 5a**, where two different regions can be defined: First, the proximity effect region for $d_\mathrm{w,norm} < 0.5$, where the fringing field of the air gap pulls the current towards the center of the conductor and second, the skin effect region for $d_\mathrm{w,norm} > 0.5$, where the fringing field of the air gap cannot compensate the skin field anymore and the current flows at the edges of the conductor only. In **Fig. 5b**, these two regions are depicted in more detail depending on the frequency f_sw for different discrete distances d_w at ①...⑥.

On the left side, the F_R-values for three different $d_\mathrm{w,norm}$ at ①...③ in the proximity region are shown. For low frequencies f_sw, the proximity losses are strongly increasing with f_sw, as

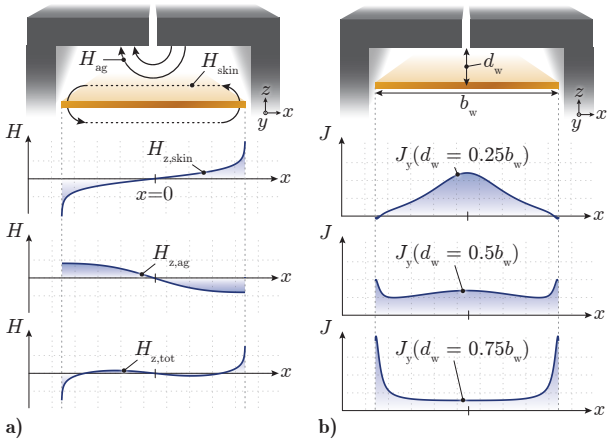

Fig. 4. a) Magnetic fields $H_\mathrm{z,skin}$, $H_\mathrm{z,ag}$ and $H_\mathrm{z,tot}$, where only their components perpendicular to the conductor surface, i.e. in z-direction, are considered. Additionally, $H_\mathrm{z,skin}$ corresponds to a homogeneous current distribution in the conductor and $H_\mathrm{z,tot} = H_\mathrm{z,skin} + H_\mathrm{z,ag}$. **b)** shows the resulting HF current densities J_y for different distances d_w between the air gap and the conductor.

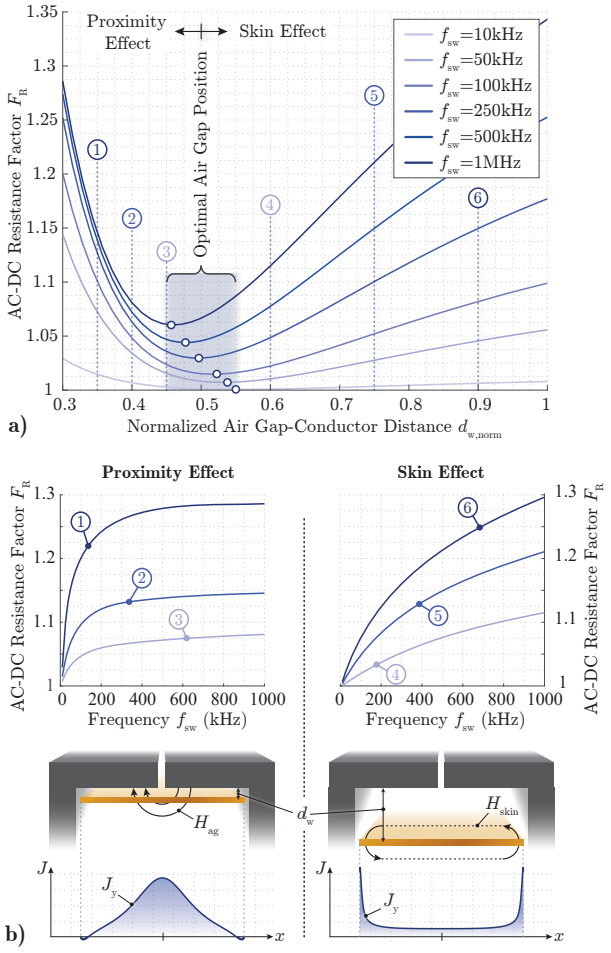

Fig. 5. a) AC to DC resistance factor F_R of a straight conductor for different values $d_{w,norm} = \frac{d_w}{b_w}$ and different frequencies f_{sw}. The optimal air gap placement for all frequencies lies around $d_{w,norm} = 0.5$, where below this value the proximity effect increases F_R and above the optimum the skin effect becomes dominant. Both effects are illustrated in **b)** for three different $d_{w,norm}$ values ①, ②, ③ and ④, ⑤, ⑥ , respectively.

the current distribution is getting more and more triangularly shaped. However, the current is pulled towards a region with a very low perpendicular magnetic field $H_{z,tot}$ (cf. **Fig. 4a**), which is why the losses do no longer significantly increase with frequency, once all the current is in this "low-field-region".

On the right-hand side, the F_R-values for the three different $d_{w,norm}$ at ④...⑥ in the skin region are shown. As the current is pushed towards the edges of the conductor, where the highest magnetic fields occur, the conduction losses are constantly increasing with frequency with the well-known $\sqrt{f_{sw}}$ dependency.

However, between the two regions, where the optimal air gap position can be found, the F_R value is less than 1.1 even for very high frequencies. Consequently, an almost homogeneous current density can be achieved, where $H_{z,tot}$ hardly affects the current distribution. As a result, a loss factor F_{H2} can be introduced

$$P_{loss} \propto \int_V H_{z,tot}^2 dV \rightarrow F_{H2} = \int_V H_{z,tot}^2 \mathrm{d}V, \tag{9}$$

as the HF losses are directly proportional to the penetrating magnetic field, as long as the current distribution in the winding does not change significantly [12]. This simple H^2-loss factor can be used to accurately predict the optimal air gap position, without carrying out a time-consuming FEM optimization. In addition, for very simple geometries, the optimum air gap position can even be found analytically. For the arrangement at hand, the H^2-loss factor and the optimal air gap position $d_{w,opt}$ can be calculated based on (6)-(8) according to

$$F_{H2} = \int_V H_{z,tot}^2 dV \xrightarrow{\text{minimize}} \frac{\partial}{\partial d_w} F_{H2} \stackrel{!}{=} 0 \tag{10}$$

and

$$\begin{aligned} \frac{\partial}{\partial d_w} F_{H2} &= \frac{\partial}{\partial d_w} \int_V H_{z,tot}^2 dV \\ &= \int_V 2 H_{z,tot} \frac{\partial}{\partial d_w} H_{z,tot} dV \\ &\rightarrow d_{w,opt} = \frac{b_w}{2}. \end{aligned} \tag{11}$$

Hence, the analytically derived optimal air gap position $d_{w,opt}$ coincides with the optimal position found based on FEM simulations (cf. **Fig. 5a**).

A possible practical implementation of a PCB winding inductor, using the proposed field compensation concept on straight winding sections, is shown in **Fig. 6a**. However, this design has significant drawbacks, as the end-winding sections are not covered by the air gap, hence the skin and proximity fields are not compensated anymore and the conduction losses in these sections significantly increase. In addition, the ratio between the winding length l_{ws} and the core area A_C is comparably poor compared to the circular arrangement shown in **Fig. 6b**. Assuming the same total core cross section A_C in both designs, the ratio between the winding lengths can be calculated according to

$$L_w(k) = \frac{l_{ws}}{l_{wc}} = \frac{1+k}{\sqrt{\pi k}}, \tag{12}$$

where k denotes the ratio between the length and the width of the core cross section A_C of **Fig. 6a**. Hence, the minimum ratio between the winding lengths can be found to be

$$\frac{\partial}{\partial k} L_w(k) \stackrel{!}{=} 0 \xrightarrow{k=1} L_w(1) = \frac{2}{\sqrt{\pi}} > 1. \tag{13}$$

Thus, even for the optimal value $k = 1$ (square cross section), the winding length of the rectangular core l_{ws} is larger than l_{wc}. Consequently, the circular arrangement of **Fig. 6b** should be used in practical applications, as in addition to the reduced winding length, the circularly shaped winding and air gap allow to compensate the skin and proximity fields along the whole winding, whereby the aforementioned end-winding losses can be avoided. However, the circular shape of the conductor might influence the optimal air gap position, which will be investigated in the following section.

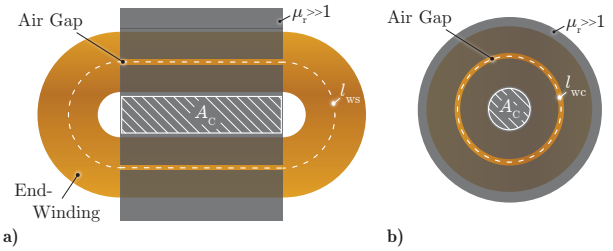

Fig. 6. a) Practical implementation of a PCB winding inductor with a partially straight winding, resulting in large end-winding losses and **b)** an improved pot core arrangement with a circular winding with minimum length.

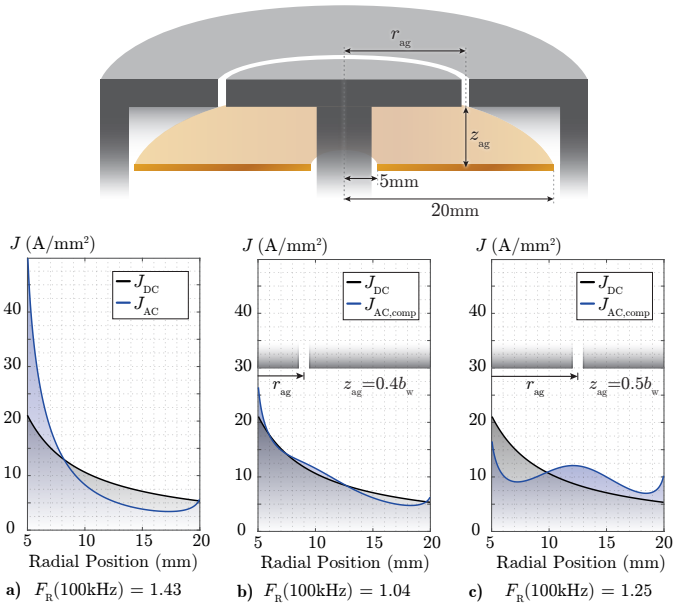

Fig. 7. Qualitative sketch of a circular PCB winding inductor arrangement (in reality, the width of the outer shell would be much smaller) and three different current distributions: **a)** DC current density J_{DC} in a circular conductor and its HF equivalent J_{AC} without an air gap in its near vicinity. **b)** DC current density and its HF counterpart $J_{AC,comp}$ with the air gap ideally positioned. **c)** DC current density and its HF counterpart $J_{AC,comp}$ with the air gap positioned in the optimal spot for a straight conductor (cf. (11)).

III. Field Compensation in Circular Conductors

Unlike in a straight conductor, the DC current density J_{DC} in circular conductors is not homogeneous anymore and can be calculated according to

$$J_{DC}(r) = \frac{I_L}{r \cdot h_{cu} \cdot \ln\left(\frac{r_{in}}{r_{out}}\right)}, \tag{14}$$

as shown in **Fig. 7a**. Hence, as already mentioned in the previous section, the HF current density J_{AC} should match J_{DC} as closely as possible in order to achieve a low F_R value. In the same figure, the current distribution J_{AC} due to the skin effect only, thus without an air gap in the near vicinity of the conductor, is illustrated. The magnetic skin field $H_{z,skin}$ pushes the current towards the center of the inductor, whereby an increased F_R value results, even for comparably low frequencies ($F_R = 1.43$ at 100 kHz). Therefore, the fringing field $H_{z,ag}$ of the air gap is again required to compensate $H_{z,skin}$

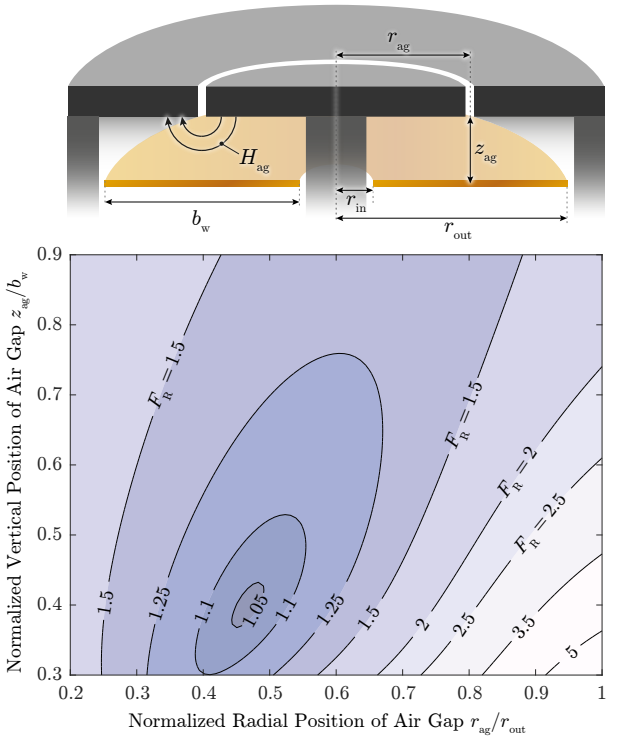

Fig. 8. AC to DC resistance factor F_R for different normalized air gap positions ($\frac{r_{ag}}{r_{out}}$, $\frac{z_{ag}}{b_w}$), a frequency of 500 kHz and a ratio of radii $\frac{r_{in}}{r_{out}}$ of 0.2.

and to pull the current away from the center of the winding to match J_{DC} as accurately as possible. The compensating effect of $H_{z,ag}$ is shown for two different air gap locations in **Fig. 7b** and **7c**, respectively.

In **Fig. 7b**, the air gap is located in the optimal position for this circular geometry, whereby a very low value for $F_R(= 1.04)$ results and $J_{AC,comp}$ hardly deviates from J_{DC}.

In **Fig. 7c**, the air gap is placed at the position which would be optimal for a straight conductor, hence in the middle of the track with a distance z_{ag} of $\frac{b_w}{2}$ (11). However, this location is far from optimal, as an almost homogeneous current distribution is achieved, which does not correspond to $J_{DC}(r)$. Consequently, the optimal air gap positions in straight and circular conductors are different and need to be calculated separately.

Once again, there are two different options to find the optimal air gap position in a circular conductor.

Either the time-consuming FEM simulation, whose results are shown in **Fig. 8** for varying z_{ag} and r_{ag} values, where z_{ag} denotes the distance between the conductor and the air gap and r_{ag} the radial position of the air gap, or by using the previously introduced H^2-loss factor F_{H2}, which is calculated based on the magnetic skin field $H_{z,skin}$ of the DC current distribution $J_{DC}(r)$ and the fringing field $H_{z,ag}$ around the air gap according to

$$J_{line}(r) = J_{DC}(r) \cdot h_{cu} = \frac{I_L}{r \cdot \ln\left(\frac{r_{in}}{r_{out}}\right)}, \tag{15}$$

$$H_{\mathrm{z,skin}}(r) = \int_{r_{\mathrm{in}}}^{r_{\mathrm{out}}} \frac{J_{\mathrm{line}}}{2\pi(r+\alpha)} \left(\frac{\alpha^2 - r^2}{(\alpha - r)^2} E(k^2) + K(k^2) \right) d\alpha,$$

$$k^2 = \frac{4\alpha r}{(\alpha + r)^2} \tag{16}$$

and

$$H_{\mathrm{z,ag}}(r) = \frac{I_{\mathrm{L}}}{\pi\sqrt{(r + r_{\mathrm{ag}})^2 + z_{\mathrm{ag}}^2}} \cdot \left(\frac{r_{\mathrm{ag}}^2 - r^2 - z_{\mathrm{ag}}^2}{(r_{\mathrm{ag}} - r)^2 + z_{\mathrm{ag}}^2} E(k^2) + K(k^2) \right),$$

$$k^2 = \frac{4 r_{\mathrm{ag}} r}{(r_{\mathrm{ag}} + r)^2 + z_{\mathrm{ag}}^2}, \tag{17}$$

where $E(k^2)$ and $K(k^2)$ denote the complete elliptic integrals of the first and second kind. The results are shown in **Fig. 9**, whereby a very close match between the results of the actual F_{R} values of **Fig. 8** and the H^2-loss factors F_{H2} can be observed. Especially for locations $(r_{\mathrm{ag}}, z_{\mathrm{ag}})$ with the lowest F_{R} values, the curves are almost identical, which allows for accurately predicting the optimal position $(r_{\mathrm{ag,opt}}, z_{\mathrm{ag,opt}})$ within a fraction of the time it would take to simulate the geometry in a FEM software.

The benefit of the significantly reduced calculation time of the H^2-loss factors cannot only be used for the previously shown straight and circular conductor arrangements, as the principle of calculating the optimal air gap position using the H^2-loss factor is very general and can be applied to all kind of winding geometries, once the DC current distribution is known.

However, in order to simplify the usage of this concept in practice, a general design guideline would be nice, which reduces the computational effort for the inductor designer.

Fortunately, in the circular arrangement of **Fig. 8**, the optimal air gap positions change with the ratio of radii only and do not depend on their absolute dimensions, which is why the desired general design guideline for circular conductors can be calculated for all ratios of radii $\frac{r_{\mathrm{in}}}{r_{\mathrm{out}}}$. The resulting optimal air gap positions $(r_{\mathrm{ag,opt}}, z_{\mathrm{ag,opt}})$ are depicted in **Fig. 10**.

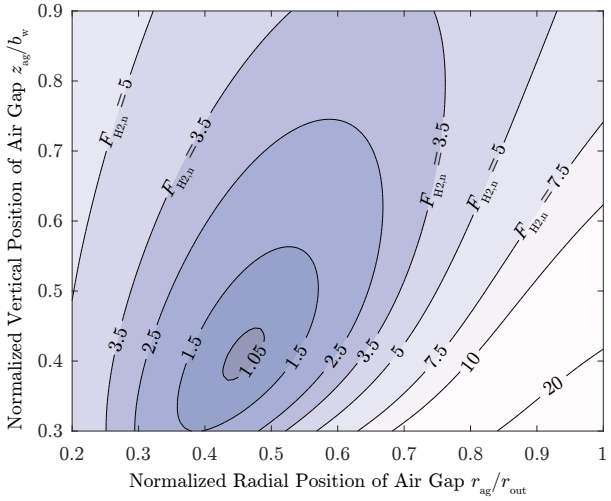

Fig. 9. Calculated normalized H^2-loss factor for the same arrangement as shown in **Fig. 8**, in order to estimate the optimal air gap position $(r_{\mathrm{ag}}, z_{\mathrm{ag}})$.

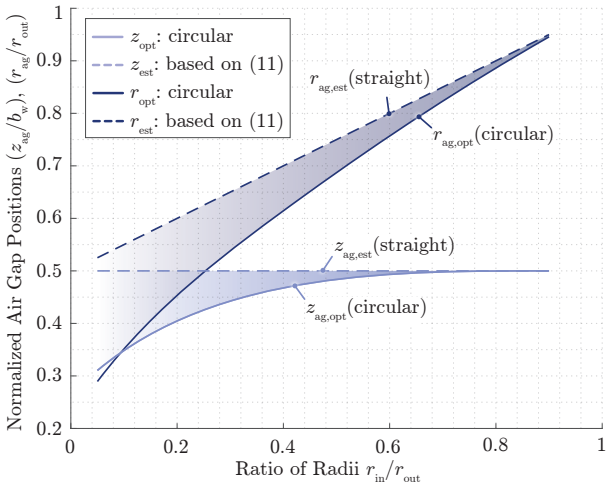

Fig. 10. Comparison between the estimated optimal air gap position based on the calculations for a straight conductor $(r_{\mathrm{ag,est}}, z_{\mathrm{ag,est}})$ and the actual optimal position based on the calculations for a circular conductor $(r_{\mathrm{ag,opt}}, z_{\mathrm{ag,opt}})$, for different ratios of radii $\frac{r_{\mathrm{in}}}{r_{\mathrm{out}}}$.

In order to illustrate the difference between the actual optimal air gap position for a circular conductor and the simplified calculation based on a straight conductor (11), the results of both calculation methods are shown. For $\frac{r_{\mathrm{in}}}{r_{\mathrm{out}}} > 0.5$, the simplified calculation $z_{\mathrm{ag,est}} = \frac{b_{\mathrm{w}}}{2}$ and $r_{\mathrm{ag,est}} = \frac{r_{\mathrm{in}} + r_{\mathrm{out}}}{2}$ yields very good results, closely following the the optimum $z_{\mathrm{ag,opt}}$ and $r_{\mathrm{ag,opt}}$ obtained from (16) and (17), as the DC current density $J_{\mathrm{DC}}(r)$ in the circular conductor is almost homogeneous. However, for lower ratios of radii, the optimal air gap position should be chosen according to the solid lines depicted in **Fig. 10**, due to the inhomogeneity of $J_{\mathrm{DC}}(r)$.

So far, only a single layer conductor has been considered. However, in practice, inductor windings usually comprise multiple turns and multiple layers in order to achieve a certain required inductance. Therefore, it is crucial to investigate the applicability of the proposed concept to multilayer windings, in order to prove its suitability for practical applications. This will be done in the following section based on a three layer arrangement.

IV. Multilayer Winding

The multilayer arrangement of **Fig. 11** comprises three PCB layers, which are all separated by thin FR4 layers (not shown in the figure). In order to calculate the F_{R} values of the three different conductors, the perpendicular magnetic fields in each layer have to be known. Thanks to the linearity of magnetoquasistatic field problems, the principle of superposition can be applied, where the magnetic fields of each source (conductors, air gap) are calculated independently and superimposed in the end. However, the calculation of the different field components is not trivial, as the complexity of the field problem is increased due to the additional dimension

in z-direction. Hence, in general, the perpendicular magnetic field throughout the PCB is not constant anymore, whereby a two-dimensional field problem would have to be solved. In order to reduce the calculation complexity of the magnetic field problem, it is assumed that the mutual distance d_L between the layers is much smaller than the width b_w of the copper tracks and therefore a constant z-component of the magnetic field $H_\mathrm{z,skin}$ throughout the height of the PCB can be presumed. However, in the multilayer arrangement at hand, the total appearing parasitic magnetic field $H_\mathrm{z,skin+prox}$ in the PCB is now induced by multiple individual layers. Thus, the magnetic skin field $H_\mathrm{z,skin,1}$ for example, which is induced by the current I_L in the top layer of the PCB, penetrates not only the top layer itself, but also the two remaining layers (middle and bottom) as proximity field $H_\mathrm{prox,1}$. The same holds true for $H_\mathrm{z,skin,2}$ and $H_\mathrm{z,skin,3}$, whereby the total parasitic magnetic field in each layer can be calculated by superposition according to

$$H_\mathrm{z,skin} = H_\mathrm{z,skin,1} + H_\mathrm{z,skin,2} + H_\mathrm{z,skin,3}. \tag{18}$$

Assuming the same DC current distribution $J_\mathrm{DC}(r)$ in all turns, the total skin field $H_\mathrm{z,skin}$ can therefore be calculated based on (16), using the equivalent line current density

$$J_\mathrm{line}(r) = \sum_{\mathrm{i}=1}^{3} J_\mathrm{line,i}(r) = \frac{3 \cdot I_\mathrm{L}}{r \cdot \ln\left(\frac{r_\mathrm{in}}{r_\mathrm{out}}\right)}. \tag{19}$$

Thus, the magnetic skin field in a three-layer winding is equivalent to the magnetic field induced by a single conductor carrying three times the inductor current I_L.
For this reason, the F_R value of each layer can be calculated separately according to **Fig. 5**, as the magnetic flux in the core and therefore the fringing field around the air gap H_ag is excited by $N \cdot I_\mathrm{L} = 3 \cdot I_\mathrm{L}$ as well. However, as the minimum distance between the different PCB layers is limited

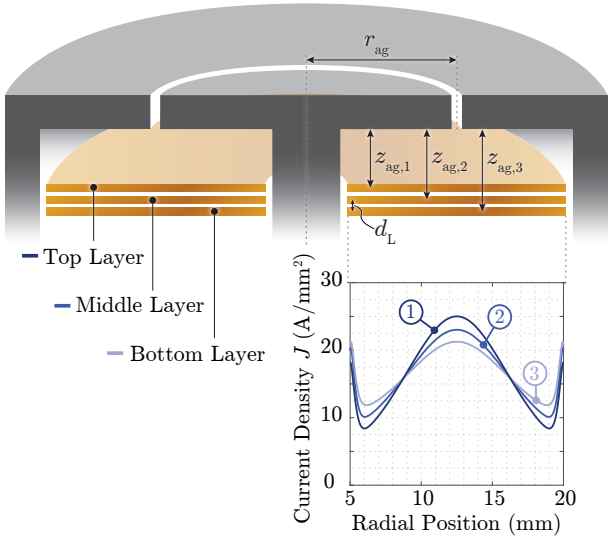

Fig. 11. Circular inductor arrangement with multiple turns on adjacent layers and their respective current densities J_AC.

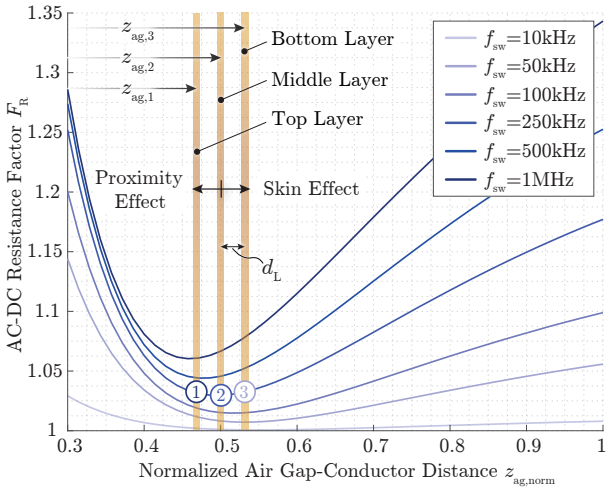

Fig. 12. F_R values for each layer in a multilayer PCB winding for different frequencies f_sw and different air gap positions $z_\mathrm{ag,norm} = \frac{z_\mathrm{ag}}{b_\mathrm{w}}$.

by manufacturing constraints, they cannot all be placed in the optimal position $z_\mathrm{ag,opt}$. Hence, two out of the three layers are either slightly under- or overcompensated as shown in **Fig. 11**. The non-ideal current densities of the two outer layers slightly affect their F_R values as illustrated in **Fig. 12**, where the top layer ① lies within the proximity effect region and the bottom layer ③ in the skin effect region, respectively. However, as long as the distance between layers d_L is much smaller than the widths b_w of the copper tracks, the F_R values of the different layers are almost the same and the calculated optimal air gap position of a single layer arrangement can also be applied to multilayer windings.
It needs to be mentioned, that the quality of the compensation highly depends on the ratio between d_L and b_w, as for large d_L values the simplified assumption of a constant vertical magnetic field throughout the PCB is not valid anymore. Hence, the full two-dimensional field problem needs to be solved, which is however out of the scope of this paper.
Nevertheless, in most designs $d_\mathrm{L} \ll b_\mathrm{w}$ is ensured and the proposed field compensation concept achieves F_R values close to one, even for multilayer windings. Thus, very efficient high frequency PCB winding inductors for all kinds of inductance values can be designed.
In **Fig. 13**, an exemplary practical implementation of such an inductor with a multilayer PCB winding is shown. It should be pointed out that, in order to minimize the termination losses in the inductor, it is crucial to terminate the winding in a coplanar way, so that a homogeneous current density in the connecting copper tracks is achieved. In addition, the transitions between the layers should be done by means of through-hole vias only, as the usage of blind and buried vias increases the manufacturing costs of PCB windings significantly.

V. Conclusion

In this paper, a new method of designing highly efficient high-frequency PCB inductor windings has been introduced, where the fringing field of a single air gap can be used

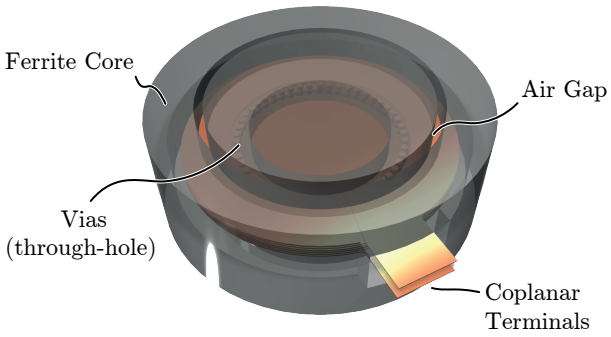

Fig. 13. Practical implementation of a PCB winding inductor, where the proposed field compensation concept is applied.

in such a way, that the existing skin and proximity fields in a PCB inductor winding are largely compensated. Thus, compared to state-of-the-art solutions, the fringing field of an air gap is not avoided anymore, but rather used to actively compensate adverse high-frequency effects ("turn enemies into friends"). Furthermore, the difficult manufacturing of multi-air-gap and low-permeability cores can be avoided, as a certain magnetic fringing field is desired. Consequently, cost-effective and efficient PCB inductor windings can be designed based on the design guidelines shown in this paper. Additionally, the proposed H^2-loss factor calculation method allows for a fast calculation of the optimal air gap position for all different kinds of geometries. Thus, the proposed field compensation concept is by far not limited to standard inductor arrangements as the ones shown in this paper.

Acknowledgment

The authors would like to thank the Robert BOSCH GmbH for supporting this work.

References

[1] A. Consoli, F. Gennaro, C. C., and A. Testa, "A comparative study of different buck topologies for high efficiency low voltage applications," in *IEEE Power Electronics Specialists Conference (PESC)*, 1999.

[2] M. Forouzesh, Y. P. Siwakoti, and B. Lehman, "Step-up dc/dc converters: A comprehensive review of voltage-boosting techniques, topologies, and applications," in *IEEE Transactions on Power Electronics, Vol. 32, No. 12*, 2017.

[3] C. R. Sullivan, "Prospects for advances in power magnetics," in *International Conference on Integrated Power Electronics Systems (CIPS)*, 2016.

[4] B. A. Reese and C. R. Sullivan, "Litz wire in the mhz range: Modeling and improved designs," in *Conference on Control and Modeling for Power Electronics (COMPEL)*, 2017.

[5] C. R. Sullivan, "Layered foil as an alternative to litz wire: Multiple methods for equal current sharing among layers," in *Conference on Control and Modeling for Power Electronics (COMPEL)*, 2014.

[6] M. Nigam and C. R. Sullivan, "Multi-layer folded high-frequency toroidal inductor windings," in *Applied Power Electronics Conference and Exposition (APEC)*, 2008.

[7] R. Wrobel, S. Ayat, and J. L. Baker, "Analytical methods for estimating equivalent thermal conductivity in impregnated electrical windings formed using litz wire," in *Electric Machines and Drives Conference (IEMDC)*, 2017.

[8] R. M. Burkart, "Advanced modeling and multi-objective optimization of power electronic converter systems," Ph.D. dissertation, ETH Zurich, 2016.

[9] J. Hu and C. R. Sullivan, "Ac resistance of planar power inductors and the quasidistributed gap technique," in *IEEE Transactions on Power Electronics, Vol. 16, No. 4*, 2001.

[10] W. A. Roshen, "Fringing field formulas and winding loss due to an air gap," in *IEEE Transactions on Magnetics, Vol. 43, No. 8*, 2007.

[11] P. Wallmeier and H. Grotstollen, "Magnetic shielding applied to high-frequency inductors," in *IEEE Industry Application Society, Annual Meeting*, 1997.

[12] M. Leibl, "Three-phase pfc rectifier and high-voltage generator for x-ray systems," Ph.D. dissertation, ETH Zurich, 2017.